Reconstruction in Diffraction Ultrasound Tomography Using Nonuniform FFT

Michael M. Bronstein*, *Member, IEEE*, Alexander M. Bronstein, *Member, IEEE*, Michael Zibulevsky, *Member, IEEE*, and Haim Azhari, *Senior Member, IEEE*

Abstract—We show an iterative reconstruction framework for diffraction ultrasound tomography. The use of broad-band illumination allows significant reduction of the number of projections compared to straight ray tomography. The proposed algorithm makes use of forward nonuniform fast Fourier transform (NUFFT) for iterative Fourier inversion. Incorporation of total variation regularization allows the reduction of noise and Gibbs phenomena while preserving the edges. The complexity of the NUFFT-based reconstruction is comparable to the frequency-domain interpolation (gridding) algorithm, whereas the reconstruction accuracy (in sense of the L^2 and the L^∞ norm) is better.

Index Terms—Acoustic diffraction tomography, image reconstruction, nonuniform fast Fourier transform (NUFFT).

I. INTRODUCTION

U LTRASOUND tomography with diffracting sources is an important type of acoustic imaging. Since the used wavelengths are comparable to the object feature dimensions, wave phenomena such as diffraction become significant. Consequently, the straight ray tomography theory is no longer applicable.

The analog of the Fourier Slice Theorem used in straight ray tomography is the Fourier Diffraction Theorem [1]–[5]. Using this theorem, image reconstruction in diffraction tomography can be considered as a problem of signal reconstruction from nonuniform frequency samples.

Reconstruction methods used previously addressed the problem as a straightforward approximation of the inverse nonuniform Fourier transform (NUFT) and involved frequency interpolation [2], which is liable to introduce significant inaccuracies. More accurate and computationally efficient methods [6]–[9] were proposed for forward and inverse one-dimensional (1-D) NUFT. Fast forward NUFT algorithms can be generalized to higher dimensions, whereas the generalization of the inverse
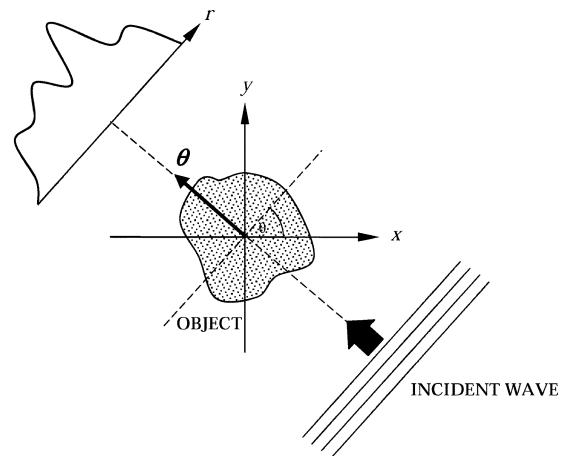
Fig. 1. Acquisition of a single projection in ultrasound diffraction tomography [2].

ones is not trivial. For this reason, we limit our work to the use of the forward nonuniform fast Fourier transform (NUFFT).

Recently, fast and accurate approximation of the forward nonuniform Fourier transform was introduced by Fessler and Sutton [10]. Inverse NUFFT can be achieved iteratively in this framework [11]. We adopt this approach for iterative reconstruction in diffraction tomography, combining it with total variation regularization [12]–[17] in order to suppress noise while preserving the sharpness of edges.

Simulation studies with the Shepp–Logan phantom show that the proposed algorithm significantly outperforms the frequency interpolation methods.

II. PRINCIPLES OF DIFFRACTION TOMOGRAPHY

Diffraction tomography allows reconstructing the refractive index $\gamma(\boldsymbol{x})$ of a scattering object by processing the data obtained in scattering experiments [18]. In the classical configuration, shown in Fig. 1, the object is illuminated with a plane acoustic wave with wave number $K = 2\pi/\lambda$ and temporal frequency $\omega = 2\pi c/\lambda$ (λ denotes the wavelength), propagating in direction $\boldsymbol{\theta}$

$$\psi_\theta(\boldsymbol{x}, t) = \exp(-i\omega t)\exp(-iK\boldsymbol{x}\cdot\boldsymbol{\theta}) \triangleq \exp(-i\omega t)u_\theta(\boldsymbol{x}).$$
(1)

The resulting field $u(\boldsymbol{x})$ satisfies the reduced wave equation

$$\Delta u(\boldsymbol{x}) + K^2(1 + f(\boldsymbol{x}))u(\boldsymbol{x}) = 0, \quad f(\boldsymbol{x}) = \gamma^2(\boldsymbol{x}) - 1 \quad (2)$$

where Δ denotes the Laplacian operator. $u(\boldsymbol{x})$ can be written as a superposition of the *incident field* $u_\theta(\boldsymbol{x})$, computed under the assumption of a homogeneous medium, and the *scattered field* $u_s(\boldsymbol{x})$, attributed solely to the inhomogeneities [2]. The scattered field is measured along a line of detectors.

Equation (2) can be rewritten in an integral form, known as the Lippmann–Schwinger integral equation

$$u_s(\boldsymbol{x}) = -K^2 \int_\Omega G(\boldsymbol{x} - \boldsymbol{y}) f(\boldsymbol{y}) u(\boldsymbol{y}) \, d\boldsymbol{y} \qquad (3)$$

where $G(\boldsymbol{x})$ is the appropriate Green function [19].

Reconstruction is possible by linearization of (3). The *Born approximation* is obtained by assuming weak scattering $(u(\boldsymbol{x}) \approx u_\theta(\boldsymbol{x}))$. The inverse problem in this case implies the solution of the integral equation

$$u_s(\boldsymbol{x}) = -K^2 \int_\Omega G(\boldsymbol{x} - \boldsymbol{y}) f(\boldsymbol{y}) u_\theta(\boldsymbol{y}) \, d\boldsymbol{y} \qquad (4)$$

which is a direct generalization of the Radon transform [19].

Under the assumption of the Born approximation, a possible alternative is solving the inverse problem in the frequency domain. The Fourier Diffraction Theorem relates the Fourier transform of the measured scattered field projection with the Fourier transform of the object.

Fourier Diffraction Theorem

Given a projection $P_\theta(r)$ of the forward scattered field $u_s(\boldsymbol{x})$ obtained by illuminating an object $f(\boldsymbol{x})$ with a plane wave, the following equation holds:

$$\mathcal{F}\{P_\theta(r)\}(\omega) = \mathcal{F}_{2D}\{f(x)\}(\boldsymbol{K}(\omega)) \qquad (5)$$

where

$$
\begin{aligned}
\boldsymbol{K} &= (K_x, K_y), \\
K_x(\omega) &= \omega \cos\theta - \left(\sqrt{K_0^2 - \omega^2} - K_0 \right) \sin\theta \\
K_y(\omega) &= \omega \sin\theta + \left(\sqrt{K_0^2 - \omega^2} - K_0 \right) \cos\theta \\
K_0 &= \frac{2\pi}{\lambda}
\end{aligned}
\qquad (6)
$$

and $\mathcal{F}$ and $\mathcal{F}_{2D}$ denote the 1-D and two-dimensional (2-D) Fourier transforms, respectively.

In other words, the Fourier transform of the projection gives the values of the 2-D Fourier transform of the object along a semicircular arc in the spatial frequency domain, as depicted in Fig. 2 [2].

Since wave phenomena obey the superposition principle, illuminating the object with a wave consisting of a set of frequencies (referred to as *broad-band illumination*), rather than a monochromatic wave, will produce samples along a set of semicircular arcs with different radii. Hence, a single projection potentially contains much more information about the object than a single projection in straight ray tomography. By taking advantage of this fact, one can achieve sufficient image quality with fewer projections.

Two main reconstruction strategies in diffraction tomography are interpolation in the frequency domain (analogous to the di-
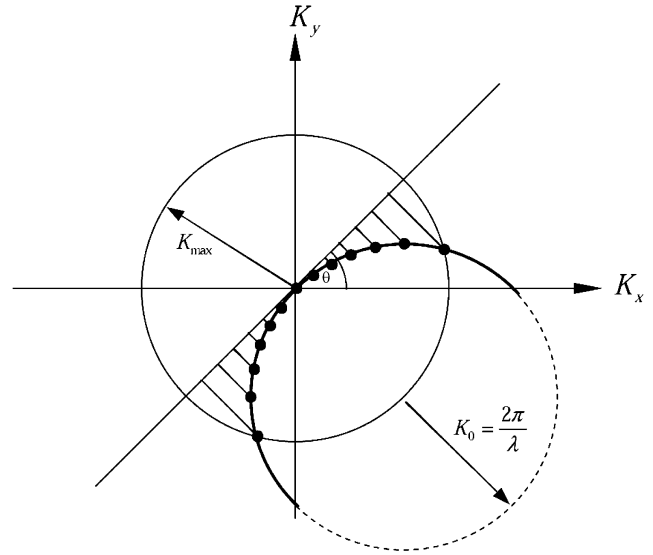

Fig. 2.   Illustration of the Fourier Diffraction Theorem.

rect Fourier inversion in straight ray tomography) and interpolation in the space domain (analogous to the filtered backprojection), usually termed *backpropagation* [4], [20]. However, unlike straight ray tomography, interpolation in the space domain is computationally extensive, and thus the majority of efficient algorithms are based on frequency-domain interpolation.

A common method of image reconstruction in the frequency domain is the gridding algorithm [2], [21]. The nonuniform data is interpolated to a uniform Cartesian grid using, for example, polynomial interpolation. Afterwards, the inverse Fourier transform is efficiently computed using FFT. However, this approach is liable to introduce inaccuracies and is sensitive to the configuration of the sample points.

In the next section, we introduce an iterative reconstruction method which allows the reconstruction of the image from nonuniform samples in the frequency domain without using gridding.

III. NUFT

The heart of iterative image reconstruction from nonuniform frequency samples is the forward NUFFT. To define the NUFFT problem, we first consider a 1-D case.

Let $\boldsymbol{\xi} = (\xi_1, \ldots, \xi_K) : \xi_k \in [-\pi, \pi]$ be a vector of nonuniformly distributed frequencies and $\boldsymbol{f} = (f_{-N/2}, \ldots, f_{N/2-1}) : f_n \in \mathbb{C}$ be a vector of samples of a signal. The nonuniform Fourier transform is defined by

$$F_k = \sum_{n=-N/2}^{N/2-1} f_n \exp(-in\xi_k). \qquad (7)$$

In matrix notation

$$\boldsymbol{F} = \Psi \boldsymbol{f} \qquad (8)$$

where $\Psi \in \mathbb{C}^{K \times N}$ $(K \geq N)$ is a full column rank matrix containing K discrete exponent functions in its rows

$$\Psi = (\boldsymbol{\psi}_1; \ldots; \boldsymbol{\psi}_K) \qquad \boldsymbol{\psi}_k(n) = \exp(-in\xi_k). \qquad (9)$$
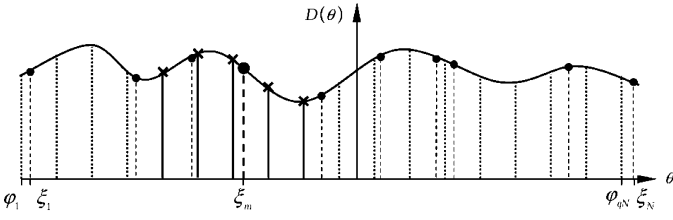
Fig. 3. Example of 1-D forward NUFFT using p neighbors. Discrete Time Fourier Transform $D(\theta)$ of the signal (solid line) is sampled at qN uniform points (dotted lines). Transform value in the nonuniform grid point ξ_m (large dot) is approximated using p uniform neighbors (crosses).

Fast approximation $\mathcal{T}$ of the NUFT operator can be achieved by projecting the signal $\boldsymbol{f}$ on some oversampled uniform Fourier basis $\Phi \in \mathbb{C}^{qK \times N}$ using standard FFT, with consequent efficient interpolation

$$\boldsymbol{F} \approx \mathcal{T}\boldsymbol{f} = U_p \Phi \boldsymbol{f} \tag{10}$$

where U_p denotes the interpolation operator, which makes use of p neighboring uniform samples for approximation of each nonuniform sample and q is the oversampling factor (see Fig. 3). The overall complexity of such an algorithm is $O(qN \log qN + pK)$.

Selecting the interpolation coefficients U_p is a problem *per se,* and there are many ways of doing it (see, for example, [22]). Recently, Fessler and Sutton [10], [11] proposed obtaining such interpolation coefficients that minimize the maximum approximation error at a given point of the nonuniform grid over all signals with unit l_2 norm. This approach can be formulated as a min–max problem

$$\min_{\boldsymbol{u}_k} \max_{\|f\|_2 \leq 1} \left| \boldsymbol{u}_k \Phi_p^k \boldsymbol{f} - \boldsymbol{\psi}_k \boldsymbol{f} \right|^2 \tag{11}$$

where $\boldsymbol{u}_k$ is the nonzero part of the kth row of the interpolation matrix U_p, and Φ_p^k is a part of the overcomplete discrete Fourier transform (DFT) basis Φ, containing p nearest neighbors of the nonuniform basis element $\boldsymbol{\psi}_k$.

Substituting explicit expression for the maximum

$$\max_{\|f\|_2 \leq 1} \left| \left(\boldsymbol{u}_k \Phi_p^k - \boldsymbol{\psi}_k \right) \boldsymbol{f} \right|^2 = \left\| \boldsymbol{u}_k \Phi_p^k - \boldsymbol{\psi}_k \right\|_2^2 \tag{12}$$

we reduce (11) to the following least squares formulation:

$$\min_{\boldsymbol{u}_k} \left\| \boldsymbol{u}_k \Phi_p^k - \boldsymbol{\psi}_k \right\|_2^2 \tag{13}$$

which has an analytic solution

$$\boldsymbol{u}_k = \boldsymbol{\psi}_\kappa \Phi_p^{k^{\mathrm{H}}} \left(\Phi_p^k \Phi_p^{k^{\mathrm{H}}} \right)^{-1} \tag{14}$$

corresponding to the coefficients of the best approximation of $\boldsymbol{\psi}_k$ in Φ_p^k (superscript H denotes Hermitian transpose). In practice, the interpolation coefficients can be precomputed. Efficient computation of the adjoint operator $\mathcal{T}^\dagger = \Phi^{\mathrm{H}} U_p^{\mathrm{H}}$, crucial for iterative optimization algorithms, is possible as well.
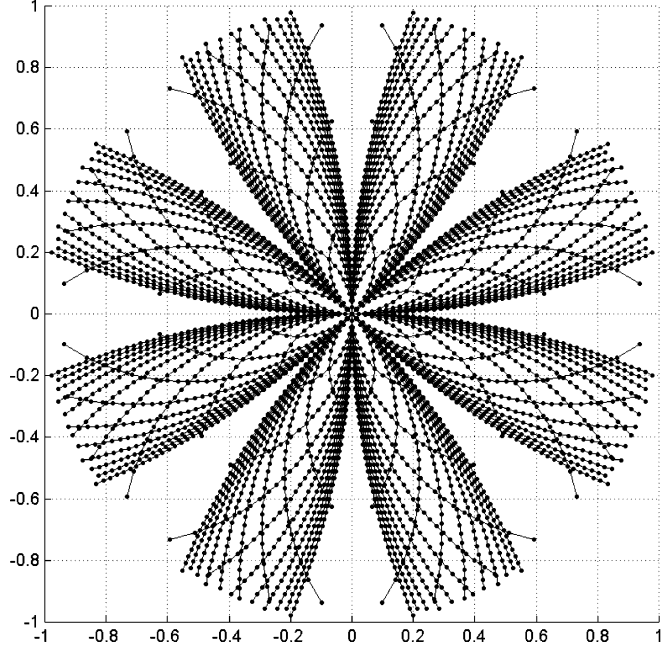

Fig. 4. Frequency-domain sampling corresponding to 8 broad-band projections (normalized spatial frequency).

IV. ITERATIVE SOLUTION OF THE INVERSE PROBLEM

A. Formulation of the Optimization Problem

A straightforward solution of the inverse problem of (8) is a computationally extensive operation. It is given by the Moore–Penrose pseudoinverse

$$\boldsymbol{f} = \Psi^+ \boldsymbol{F} = \left(\Psi^{\mathrm{H}} \Psi \right)^{-1} \Psi^{\mathrm{H}} \boldsymbol{F}. \tag{15}$$

However, such a solution is practically impossible when N is large, since it requires inversion of a $N \times N$ matrix in the 1-D case and of a $N^2 \times N^2$ matrix in the 2-D case ($O(N^3)$ and $O(N^6)$ operations, respectively).

Alternatively, (8) can be reformulated as an optimization problem

$$\min_f \|\mathcal{T}\boldsymbol{f} - \boldsymbol{F}\|_2^2. \tag{16}$$

It is possible to add a penalty on some kind of signal irregularity to the object function

$$\min_f \|\mathcal{T}\boldsymbol{f} - \boldsymbol{F}\|_2^2 + \mu\varphi(\boldsymbol{f}) \tag{17}$$

where μ is a parameter controlling the influence of the penalty. Such a penalty approach is usually referred to as Tikhonov regularization [17].

This problem can be solved iteratively using various large-scale optimization techniques, which require efficient computation of the objective function and its gradient [23]. Computation of the gradient of the cost function $g(\boldsymbol{f})$ in (17), given by

$$\nabla g(\boldsymbol{f}) = 2\mathcal{T}^\dagger (\mathcal{T}\boldsymbol{f} - \boldsymbol{F}) + \mu\nabla\varphi(\boldsymbol{f}) \tag{18}$$

exploits the fast forward operator $\mathcal{T}$, and its adjoint $\mathcal{T}^\dagger$.

In this paper, we used the conjugate gradient (CG) method with Fletcher–Reeves update formula and cubic line search to
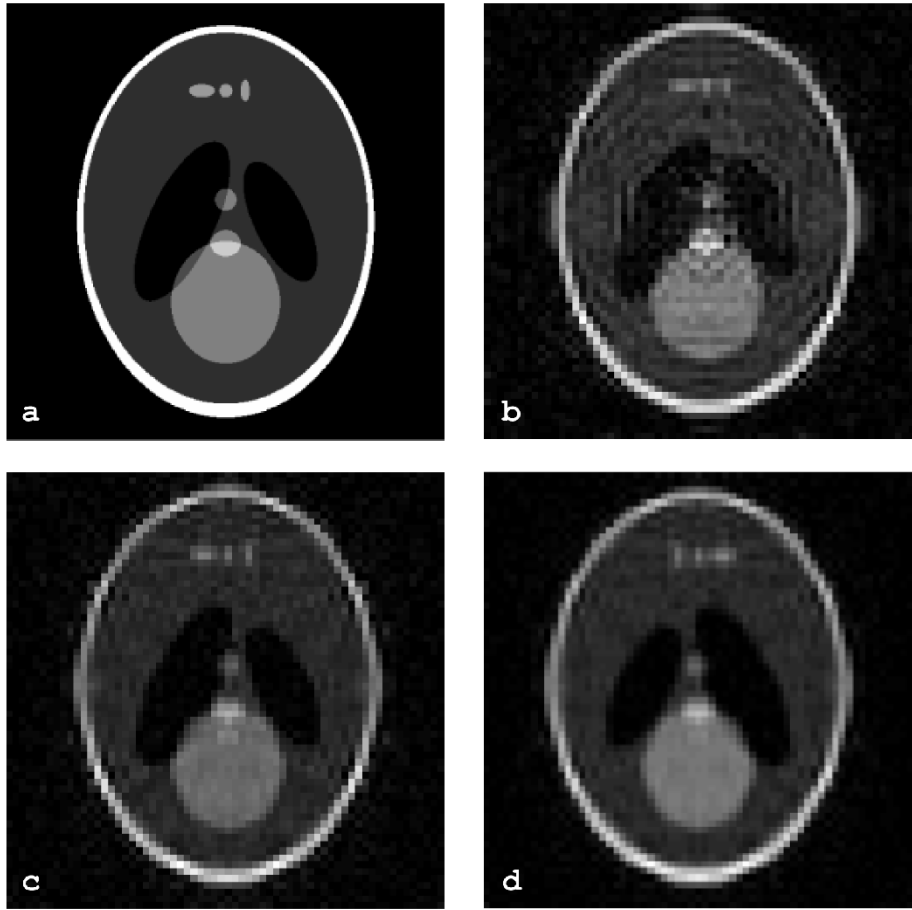
Fig. 5.   (a) Original band-unlimited phantom. (b) Reconstruction by gridding. (c) Iterative least squares reconstruction. (d) Iterative reconstruction with total variation penalty ($\mu = 100$).

solve the optimization problem (see [23] for the algorithm description).

B. Total Variation Regularization

Empirical observations show that the majority of images that occur in nature, and particularly in medical imaging applications, belong to the class of functions of bounded total variation (defined as the integral of the gradient l_2 norm) [24].

The penalty term for total variation can be used in (17). For a discrete image, the total variation is given by

$$\mathrm{TV}(\boldsymbol{f}) = \sum_{i,j} \sqrt{(\boldsymbol{f}_x)_{ij}^2 + (\boldsymbol{f}_y)_{ij}^2} \qquad (19)$$

where $\boldsymbol{f}$ is the estimated discrete image being found during the iterative process and $\boldsymbol{f}_x$, $\boldsymbol{f}_y$ are its discrete directional derivatives.

Since this function is not smooth, which can be an obstacle for smooth optimization techniques, by adding a small positive smoothing parameter η, we finally get the smoothed total variation penalty

$$\varphi(\boldsymbol{x}) = \sum_{i,j} \sqrt{(\boldsymbol{f}_x)_{ij}^2 + (\boldsymbol{f}_y)_{ij}^2 + \eta}. \qquad (20)$$

The gradient of the total variation penalty term is given by

$$\nabla_{f_{i,j}} \varphi = \lambda \left[\varphi_{i-1,j}^x - \varphi_{i,j}^x - \varphi_{i,j}^y + \varphi_{i,j-1}^y \right] \qquad (21)$$

where

$$\varphi_{i,j}^x = \frac{(\boldsymbol{f}_x)_{i,j}}{\sqrt{(\boldsymbol{f}_x^2)_{i,j} + (\boldsymbol{f}_y^2)_{i,j} + \eta}}$$

$$\varphi_{i,j}^y = \frac{(\boldsymbol{f}_y)_{i,j}}{\sqrt{(\boldsymbol{f}_x^2)_{i,j} + (\boldsymbol{f}_y^2)_{i,j} + \eta}}. \qquad (22)$$

Total variation regularization removes small oscillations resulting from noise and Gibbs phenomena, without significantly affecting the edges.

V. IMPLEMENTATION

A. Stopping Condition

Consider a vector $\hat{\boldsymbol{F}} = \boldsymbol{F} + \boldsymbol{n}$ of K samples in the frequency domain contaminated by additive Gaussian noise $\boldsymbol{n} \sim \mathbb{N}(0, \sigma^2)$. We assume that the noiseless data are consistent, i.e., there exists such an optimal image $\boldsymbol{f}_0$ so that $\|\mathcal{T}\boldsymbol{f}_0 - \boldsymbol{F}\|_2^2 = 0$. Hence

$$\left\| \mathcal{T}\boldsymbol{f}_0 - \hat{\boldsymbol{F}} \right\|_2^2 = \|0 - \boldsymbol{n}\|_2^2 = \|\boldsymbol{n}\|_2^2 \approx K\sigma^2. \qquad (23)$$

The stopping condition of the optimization algorithm is derived from (23). Assuming the noise variance σ^2 to be known, the algorithm should be stopped when

$$\|\mathcal{T}\boldsymbol{f} - \boldsymbol{F}\|_2^2 \leq K\sigma^2. \qquad (24)$$

B. Selection of the Regularization Parameter μ

The unconstrained problem (17) can be formulated as a constrained problem

$$\min_{f} \varphi(\boldsymbol{f}) \qquad \text{s.t.} \ \|\mathcal{T}\boldsymbol{f} - \boldsymbol{F}\|_2^2 \leq \varepsilon \qquad (25)$$

where ε is the maximum allowed discrepancy between the given and the reconstructed data. Assuming as previously that the data is contaminated by additive Gaussian noise, and an estimate for the noise variance σ^2, a good selection would be $\varepsilon = K\sigma^2$.

The optimal value for the regularization parameter μ is the reciprocal of the Lagrange multiplier in the constrained problem (25). This value can be obtained by finding the optimum $\boldsymbol{f}^*$ of (17) with different μ and selecting the value of μ so that $\|\mathcal{T}\boldsymbol{f}^* - \boldsymbol{F}\|_2^2 \approx K\sigma^2$. In practice, one can find the regularization parameter empirically, depending on the noise level and the image contrast [16].

C. Complexity Analysis

For simplicity, we analyze the nonregularized version of the NUFFT algorithm. We assume that the iterations are carried out by the CG algorithm.

Given an $N \times N$ image, each iteration requires the cost function and its gradient to be computed, exploiting the operators $\mathcal{T}$ and $\mathcal{T}^\dagger$. Each of these operators is applied once per iteration, hence, the complexity of each iteration is $4qN^2 \log qN + 2pN^2$, where q is the oversampling constant (usually about 2) and p is the number of neighbors used for interpolation (usually about 6–8).[1]

Assuming m iterations carried out, the overall complexity is $4mqN^2 \log qN + 2mpN^2$. Practically, m is small (about 5–10) since only a few iterations are required for algorithm convergence.

For comparison, the gridding method requires $2N^2 \log N + kN^2$ operations, attributed to the 2-D inverse fast Fourier transform (IFFT) computation and frequency-domain interpolation (k is a constant depending on the interpolation method, usually about 3–6). The complexity of backpropagation is higher, about $2N^3 \log N$ [2], [25].

For 256×256 images, gridding would require about 1.3×10^6 operations and a single NUFFT iteration about 5×10^6, whereas backpropagation would require about 250×10^6 operations. Direct Fourier inversion by computing the pseudoinverse requires over 2×10^{14} operations and is not practical.

VI. SIMULATIONS

A. Shepp–Logan Phantom

In order to avoid forward-projection errors, we used an analytic Shepp–Logan phantom. The advantage of such a phantom is that its Fourier transform has a simple analytical expression.

The choice of the number of projection and frequencies was guided mainly by sampling regularity and completeness of the nonuniform Fourier basis. Since scan time is proportional to the number of projections, the goal was to select the minimal
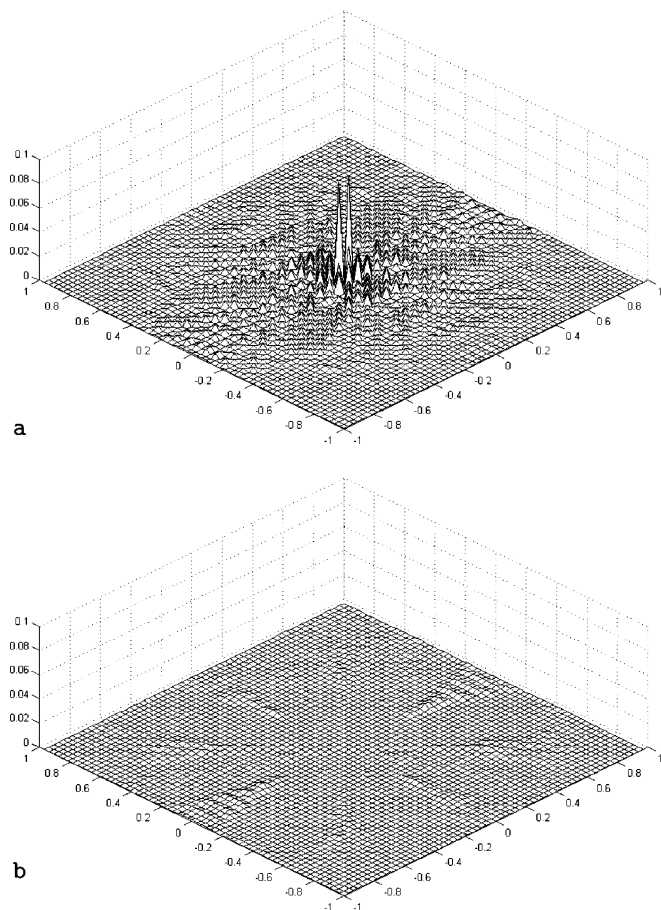

Fig. 6. Magnitude of error in the frequency domain of an image reconstructed (a) using gridding, and (b) using NUFFT.

number of projections possible that gives sufficiently regular coverage of the frequency domain. The number of samples K must be sufficiently large so the data is complete or overcomplete, i.e., $K \geq (1/2)N^2$ for real images and $K \geq N^2$ for complex ones. 64×64 images were reconstructed from eight simulated broad-band projections. Each projection contained ten frequencies $\omega_n = 0.25 \cdot \omega_0 n;\ n = 1, \ldots, 10$ (where $\omega_0 = 2\pi \times 10^7$ rad/s is the Nyquist frequency, typical for medical acoustic imaging). Frequency-domain sampling is shown in Fig. 4.

For comparison, in similar conditions, a conventional filtered backprojection (FBP) would require about 100 straight ray projections for good reconstruction of a 64×64 image [26].

B. Comparison Between Gridding and Iterative Reconstruction

The standard gridding algorithm [1] involving frequency interpolation was compared to iterative reconstruction. Nonuniform frequency samples were interpolated on a 64×64 uniform Cartesian grid using cubic polynomial interpolation and then inverted by IFFT.

Fessler's NUFFT,[2] given by (10) and (14), was used as the forward operator in iterative reconstruction carried out by the CG algorithm. Initial image was set to zero. Sufficient image

---

[1]In the regularized version of the algorithm, the iteration complexity increases about three times due to the use of linear search.

[2]The MATLAB code is available from http://www.eecs.umich.edu/~fessler, courtesy of J. Fessler.
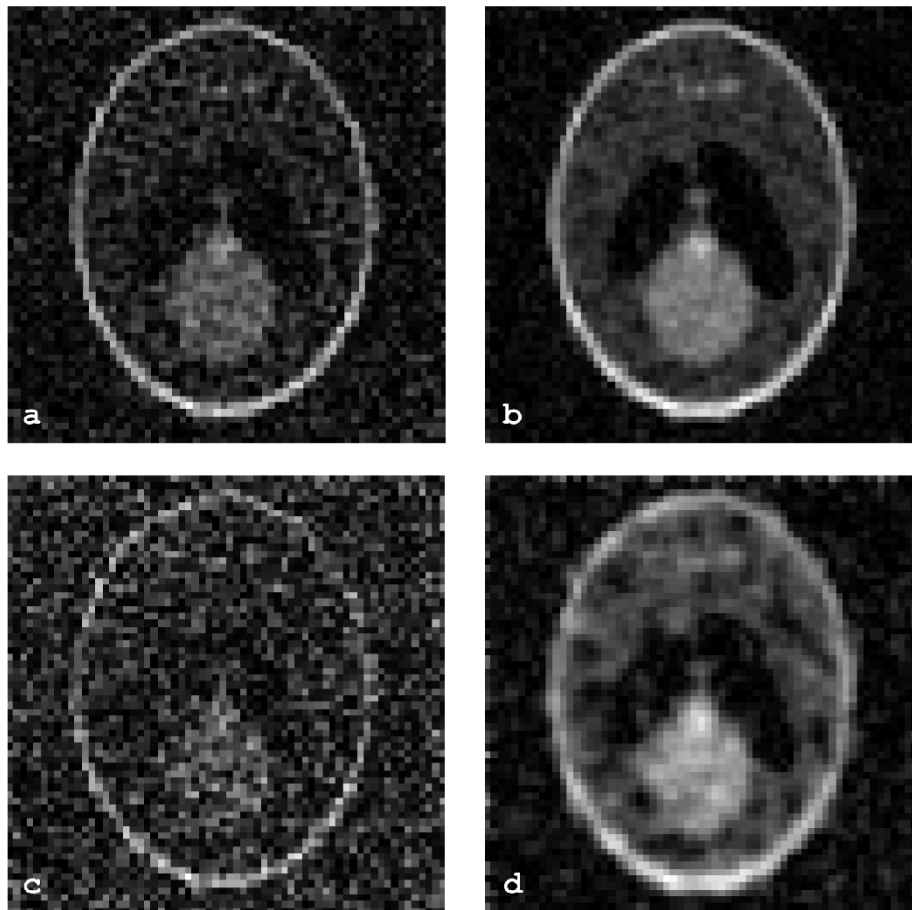
Fig. 7.   Iterative reconstruction in presence of noise. (a), (b) Signal-to-noise ratio is 20 dB. (c), (d) signal-to-noise ratio is 10 dB. Total variation penalty (b), (d) $\mu = 100$ and (a), (c) without penalty.

quality was obtained after eight iterations, using about three computations of $\mathcal{T}$ and $\mathcal{T}^\dagger$ per iteration.

Fig. 5 depicts the reconstruction results. It can be seen that unlike iterative reconstruction, the use of gridding introduces artifacts.

Interpolation in the frequency domain appears to be highly influenced by the irregularity of the frequency sampling (see Fig. 4). Since computation of the Cartesian grid points is done by interpolating the neighbor points of the nonuniform grid, sparse coverage of some regions of the frequency domain results in inaccurate interpolation. The consequences of this fact can be seen in Fig. 6, which depicts the frequency-domain error magnitude.

Iterative reconstruction appeared to be more accurate than gridding. Root-mean-square (rms) error in the frequency domain of the iterative algorithm (with respect to the analytic phantom) was about five times lower compared to gridding.

C. Influence of Total Variation Regularization

Tests were performed to study the influence of total variation regularization. Fig. 5 shows the results of the reconstruction without the regularizing term [Fig. 5(c)] and with total variation regularization [Fig. 5(d)]. In the image reconstructed without regularization, Gibbs phenomena are notable. These effects are inevitable, since the phantom has an infinite support in

the frequency domain, whereas the image is reconstructed from band-limited sampling.

When introducing the total variation penalty term, small artifacts of oscillatory nature are first to disappear. However, a too-strong penalty is liable to affect small features in the image.

The influence of total variation regularization is especially significant in the presence of noise. Fig. 7 shows images reconstructed from data contaminated by additive Gaussian noise with different variance. One can observe that the total variation penalty improves the image quality, while preserving the edges.

VII. CONCLUSION

We showed an iterative reconstruction algorithm for ultrasound tomography with diffracting sources based on min–max NUFFT. The presented method is capable of taking advantage of broad-band illumination and requires fewer projections for image reconstruction. It appeared significantly more accurate compared to the common gridding method (in sense of the L^2 and the L^∞ norm of the frequency-domain error magnitude). On the other hand, the asymptotic complexity of the NUFFT-based reconstruction is similar to gridding ($O(N^2 \log N)$ operations).

Total variation regularization has an effect of edge-preserving denosing. It allows suppression of noise and Gibbs phenomena

without significantly affecting the edges. Simulation results showed that incorporation of the total variation penalty improves the reconstruction quality in presence of noise.

Possible developments of the iterative approach can be generalization of the regularizer for other classes of signals, incorporation of different NUFFT implementations, and nonsmooth optimization techniques for efficient minimization of functions with nonsmooth penalty terms.

REFERENCES

[1] X. Pan, "A unified reconstruction theory for diffraction tomography, with consideration of noise control," *J. Opt. Soc. Amer.*, vol. 15, pp. 2312–2326, 1998.

[2] A. C. Kak and M. Slaney, *Principles of Computerized Tomographic Imaging*. Philadelphia, PA: SIAM, 2001.

[3] X. Pan, "Consistency conditions and linear reconstruction methods in diffraction tomography," *IEEE Trans. Med. Imag.*, vol. 19, pp. 51–54, Jan. 2000.

[4] A. J. Devaney, "A filtered backpropagation algorithm for diffraction images," *Ultrason. Imag.*, vol. 4, pp. 336–350, 1982.

[5] R. K. Mueller, M. Kaveh, and G. Wade, "Reconstructive tomography and applications to ultrasonics," *Proc. IEEE*, vol. 67, pp. 567–587, 1979.

[6] G. Beylkin, "On the fast Fourier transform of function with singularities," *Appl. Comput. Harmon. Anal.*, vol. 2, pp. 363–381, 1995.

[7] A. Dutt and V. Rokhlin, "Fast approximate Fourier transforms for nonequispaced data," *SIAM J. Sci. Comput.*, vol. 14, no. 6, pp. 1368–1393, Nov. 1993.

[8] ——, "Fast approximate Fourier transforms for nonequispaced data II," *Appl. Comput. Harmon. Anal.*, vol. 2, pp. 85–100, 1995.

[9] A. J. W. Duijndam and M. A. Schonewille, "Nonuniform fast Fourier transform," *Geophys. Online*, Feb. 1999.

[10] J. Fessler and B. P. Sutton, "Nonuniform fast Fourier transforms using $\mathrm{min}-\mathrm{max}$ interpolation," *IEEE Trans. Signal Process.*, to be published.

[11] J. A. Fessler, "Iterative tomographic image reconstruction using nonuniform fast Fourier transforms," Commun. Signal Process. Lab., Dept. Elect. Eng. Comput. Sci., Univ. Michigan, Ann Arbor, MI, Tech. Rep., 2001.

[12] L. I. Rudin, S. Osher, and E. Fatemi, "Nonlinear total variation based noise removal algorithms," *Phys. D*, vol. 60, pp. 259–268, 1992.

[13] P. Blomgren, T. F. Chan, P. Mulet, and C. K. Wong, "Total variation image restoration: Numerical methods and extensions," in *Proc. Int. Conf. Image Processing*, vol. 3, 1997, pp. 384–387.

[14] E. Jonsson, S. C. Huang, and T. Chan. (1998) Total variation regularization in positron emission tomography. University of California, Los Angeles, Comput. Appl. Math. Rep. 98-48. [Online]. Available: http://www.math.ucla.edu/applied/cam

[15] P. Kisilev, M. Zibulevsky, and Y. Y. Zeevi, "Total variation and wavelet regularization methods in emission tomography," Technion—Israel Institute of Technology, Haifa, Israel, Res. Rep.

[16] T. F. Chan and P. Mulet, "On the convergence of the lagged diffusivity fixed point method in total variation image restoration," *SIAM J. Numer. Anal.*, vol. 36, no. 2, pp. 354–367, 1999.

[17] C. R. Vogel and M. E. Oman, "Iterative methods for total variation denoising," *SIAM J. Num. Anal.*, vol. 17, pp. 227–238, 1996.

[18] G. A. Tsihrintzis and A. J. Devaney, "Application of a maximum likelihood estimator in an experimental study in ultrasonic diffraction tomography," *IEEE Trans. Med. Imag.*, vol. 12, pp. 545–554, Sept. 1993.

[19] Institute of Med Board on Biobehavioral Sciences and Mental Disorders, Committee on Mathematics and Physics of Emerging Dynamic Biomedica, *Mathematics and Physics of Emerging Biomedical Imaging*. Washington, DC: National Academy Press, 1996.

[20] X. Pan and M. A. Anastasio, "On a limited-view reconstruction problem in diffraction tomography," *IEEE Trans. Med. Imag.*, vol. 21, pp. 413–416, Apr. 2002.

[21] F. T. A. W. Wajer, R. Lethmate, J. A. C. van Osch, D. Graveron-Demilly, M. Fuderer, and D. van Ormondt, "Interpolation from arbitrary to Cartesian sample positions: Gridding," in *Proc. ProRISC/IEEE Workshop*, 2000, pp. 571–577.

[22] A. F. Ware, "Fast approximate Fourier transforms for irregularly spaced data," *SIAM Rev.*, vol. 40, no. 4, pp. 838–856, Dec. 1998.

[23] D. P. Bertsekas, *Nonlinear Programming*, 2nd ed. Belmont, MA: Athena Scientific, 1999.

[24] S. Mallat, *A Wavelet Tour of Signal Processing*, 2nd ed. New York: Academic, 1999.

[25] S. X. Pan and A. C. Kak, "A computational study of reconstruction algorithms for diffraction tomography: Interpolation versus filtered backpropagation," *IEEE Trans. Acoust., Speech Signal Processing*, vol. 31, pp. 1262–1275, Oct. 1983.

[26] M. Bronstein, A. Bronstein, and M. Zibulevsky. (2002) Iterative reconstruction in diffraction tomography using NUFFT. Res. Rep., Dept. Elect. Eng., Technion—Israel Institute of Technology, Haifa, Israel. [Online]. Available: http://visl.technion.ac.il/bron/works